Multiphysical simulation of bi-material nano-second laser ablation

M. DAL[a], L. CARVALHO[b], A. SEMEROK[b], W. PACQUENTIN[b],H. MASKROT[b]

a. Laboratoire PIMM, Arts et Métiers, CNRS, Cnam, HESAM Université, 151 Bd de l'hôpital 75013 Paris, France, ENSAM (morgan.dal@ensam.eu)
b. CEA, DEN/DANS/DPC/SEARS/LISL, F-91191 Gif-sur-Yvette, France(luisa.simao.carvalho@gmail.com)

Résumé :

Dans le domaine des applications laser, le traitement de surface fait l'objet de nombreuses études. Cependant, il est possible de distinguer deux sous familles basées sur les technologies laser utilisées. Citons en premier lieu les procédés à très faibles temps d'impulsion (femto ou pico secondes) connus pour leurs effets thermiques macroscopiques négligeables et leur très bonne résolution spatiale de traitement. Il est possible de trouver, en second lieu, des procédés à plus forts temps d'interaction (nano seconde) dont les cadences sont généralement meilleures et qui sont donc plus favorables aux utilisations industrielles de grandes ampleurs.

La présente étude se place dans ce dernier cas et porte sur la simulation thermo-hydrodynamique de l'ablation en régime impulsionnel nano seconde. Ce procédé, proche du perçage mais à très faible rapport de forme repose sur la vaporisation totale ou partielle de la couche superficielle du matériau à traiter. Les temps d'impulsion étant malgré tout relativement courts, les analyses expérimentales restent difficiles et généralement plutôt macroscopiques. Par conséquents, les mécanismes d'enlèvement de matière ne sont pas encore parfaitement identifiés. Citons par exemple les phénomènes d'explosion de phase liquide, de fracture mécanique ou de simple vaporisation. Les auteurs proposent donc une étude numérique visant à déterminer les mécanismes d'ablation présents pour une gamme paramétrique donnée. Pour ce faire, une simulation multiphysique est développée et dans laquelle sont intégrés les phénomènes de transferts thermiques, de mécanique des fluides, de frontière libre et de diffusion d'espèces chimiques.

Abstract :

In the field of laser applications, surface treatement is hightly studied. Two process categories are commonly used. First processes use very short pulses (femto or pico seconds) known to avoid thermal effects and to have high spatial resolutions. Second processes with higher interaction times (nano seconds) with higher treatment rates and more suitable for industry.

The current study concerns nano seconds laser technology and more precisely, the multiphysics simulation of ablation phenomenon. This process, close to drilling but with very small aspect ratios, is based on total or partial vaporization of an oxide layer to be treated. As the characteristic times still very smalls,

experimental studies are quite difficults and mainly at large scale (lot of pulses). The suposed ablation phenomena are phase explosion, mechanical fracturing and vaporization. Authors propose a numerical study that aims to identify the most laikely phenomenon leading to an oxide layer removal. To do this, a multiphysical simulation is done including heat transfers, fluid flows with free boundary and chemical species diffusion.

Key words : Laser ablation, Numerical simulation, Steel, Oxide, Vaporization

1   Introduction

Among the new cleaning processes, laser ablation technique generate a great interest since 1990 and has led to industrial patents [1, 2, 3]. Number of studies have been done on this topic in United States, France, China, Japan and United Kindom. This process is based on ejection of contaminated matier consequently to energy absorption coming from laser pulses. After ablating, the matier can be collected by vacuum and insulated to avoid environment contanimation. As this is a non contact method, the treament can be provided safely regarding contamination and as only oxide is ablated, the contamined material amount to be treated remains quite weak. Moreover, this techniques is particularly suitable for metallic treatment due to its ability to the laser beam to interact only with the contamined oxide. In these conditions, the laser ablation leads to high cleaning rate [4, 6].

Nevertheless, the process has to be optimized to reduce the residual contamination level. Indeed, litterature indicates several parameters limiting the treatment efficiency. One of the negative effect is the diffusion of contaminant in the bulk due to the laser heating [6] and the entrapment of contaminant in surface defects [5, 7, 8]. Both of them need an increase of the laser decontamination knowledge mainly treated experimentally at this time.

In addition to an experimental study, authors propose in this paper a numerical analysis of the process. To reduce the scale of the numerical problem, a single pulse is studied but results will be extrapolated to real treament conditions. The physical model and numerical assumtions will be firstly explained. After result validation, an analysis of ablation mecanisms will be proposed.

2   Physical and numerical models

In order to be sufficiently predictive for understanding, the present model has to consider heat transfers in both phases, fluid flow and mass transfers. Moreover, as the geometry is evaporating, a recoil pressure is applied at the liquid-gas boundary and the liquid boundary motion has to be considered numerically. All these phenomena will be described in the next subsections.

2.1   Geometrical assumptions

As the laser beam is circular and the workpiece quite large regarding the beam size R_0, it is possible to consider the problem in cylindrical coordinates system. Moreover, for this understanding stage, the study is focused on a single laser impact.
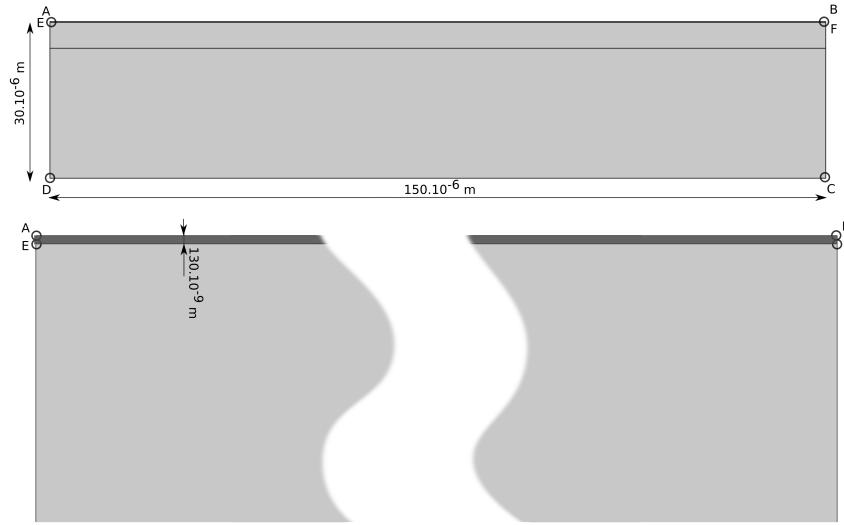
FIGURE 1 – Simulated geometry ($304L$ Stainless Steel : clear gray, Fe_3O_4 Iron Oxide : dark gray).

2.2   Mathematical models

2.2.1   Heat transfers

$$\rho_m c_{p_m}^{eq}\frac{\partial T}{\partial t} + \rho_m c_{p_m}\vec{v}.\vec{\nabla}T = \vec{\nabla}.(\lambda_m\vec{\nabla}T) + S_m(r,z,t) \tag{1}$$

Where ρ_m, c_{p_m} and λ_m are the material dependent thermal properties. T is the computed temperature and $S_m(r,z,t)$ the laser bulk power absorption set only in the oxide layer. The exponent ^{eq} indicates that the fusion latent heat is included in an equivalent [9] specific heat (eq. 2)

$$c_{p_m}^{eq} = c_{p_m} + \frac{L_m}{\sqrt{\pi\Delta T^2}}exp^{(\frac{(T-T_m)^2}{\Delta T^2/2})} \tag{2}$$

As the oxide is not perfectly opaque, a certain amount of power is distributed in the oxide bulk. This absorption is assumed to follow a Beer-Lambert law :

$$S_m(r,z,t) = \varphi_{laser}(r,t) * exp^{-(A_{Fe_3O_4}(z-z_0))} * A_{Fe_3O_4}$$

With $A_{Fe_3O_4}$ the oxide volume absorption, z_0 the z coordinate of E and F points (figure 1). φ_{laser} is the spatial and temporal distribution of the laser beam.

$$\varphi_{laser}(t) = D(t)\frac{\alpha P_m}{2f\tau\pi R_0^2}exp^{-r^2/(2R_0^2)}$$

$D(t)$ is the time distribution of the laser impulsion shown in figure 2 and coming from experimental measurements. P_m is the mean value of laser power, R_0 the standard deviation of its Gaussian expression, f the frequency and τ the pulse time duration.

Boundary conditions :
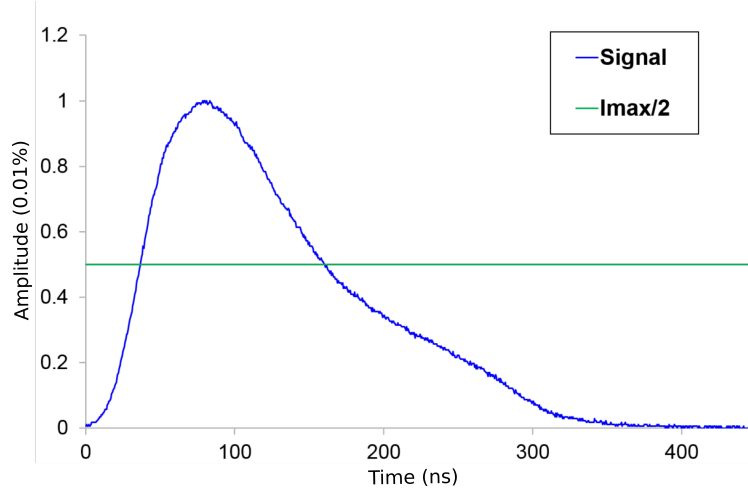
FIGURE 2 – Measured time distribution of laser power D(t).

— at $[AE] \cup [ED]$ the axial symmetry is written :

$$-\lambda_m \frac{\partial T}{\partial n} = 0$$

— at $[AB]$ the convection, radiation and evaporation heat losses are :

$$-\lambda_m \frac{\partial T}{\partial n} = -h_{cv}(T - T_\infty) - \epsilon\sigma(T^4 - T_{p,\infty}^4) - \dot{m}L_{vap}$$

— for all the other boundaries, a thermal insulation is assumed :

$$-\lambda_m \frac{\partial T}{\partial n} = 0$$

Where, h_{cv} is a convection coefficient, ϵ is the material emissivity, σ the Stefan-Boltzmann constant, $\dot{m}$ is the evaporation rate coming from Hertz-Langmuir equation [13] and L_{vap} the latent heat of vaporization.

$$\dot{m} = p_{sat}(T)\sqrt{\frac{M}{2\pi RT}}(1 - \beta_r)$$

With p_{sat} the saturation pressure (Clausius-Clapeyron equation [13]) :

$$p_{sat} = p_0 \exp^{\frac{ML_v}{R}\left(\frac{1}{T_v} - \frac{1}{T}\right)}$$

T_v is the boiling point, M the molar mass and p_0 the ambiant pressure.

2.2.2 Fluid Flow

The fluid flow problem is computed through the resolution of two equations : Momentum conservation (eq. 3) and mass conservation (eq. 4).

$$\rho_m\left[\frac{\partial\vec{v}}{\partial t} + (\vec{v}.\vec{\nabla})\vec{v}\right] = \nabla.\left(p\mathbf{I} + \mu_m(\vec{\nabla}\vec{v} + \vec{\nabla}\vec{v}^T)\right) + \vec{f}_v \tag{3}$$

$$\vec{\nabla}.\vec{v} = 0 \tag{4}$$

Where the dynamic viscosity μ_m is considered similar in both materials. It should be noted that the mass conservation is written here for a not compressible material and Boussinesq aproximations are not made here due to the very fast time dynamics avoiding convective eddies.

The boundary conditions are :
— at $[AE] \cup [ED]$ the condition is also symmetry :

$$\vec{v}.\vec{n} = 0$$

— at $[AB]$ the surface tension and the recoil pressure due to metal vaporization :

$$\sigma.\vec{n} = \gamma(T)\kappa + p_{rec}$$

— for all the other boundaries, the velocity is assumed to be zero :

$$\vec{v} = \vec{0}$$

With γ the material surface tension, κ the local curvature of the interface and p_{rec} the recoil pressure coming from the saturation pressure (eq. 5) and considering the retro-diffusion coefficient β_r [12].

$$p_{rec} = p_0 + p_{sat}\frac{(1 + \beta_r)}{2} \tag{5}$$

To complete the description, the initial conditions in velocity is zero and the pressure is set to the atmospheric one. The laser evaporation thermal and mechanical phenomena are described in more detail in litterature [10, 11, 13].

2.2.3 Species diffusion and transport

As the problem is multi-material, the proportion of each element has to be computed. The model used here is the component conservation thanks to the Fick law :

$$\frac{\partial C}{\partial t} + \vec{v}.\vec{\nabla}C = \vec{\nabla}.(D(T)\vec{\nabla}C) \tag{6}$$

For the whole boundaries, no material flux are considered. The diffusion coefficient $D(T)$ is assumed to be temperature dependent through an Arrhenius law in the solid phase and related to the Stokes-Einstein approximation in the liquide [14] :

$$
\begin{aligned}
D(T) &= D_0 exp^{(-Q/(RT))} \quad && (T < Tm_{Fe_3O_4}) \\
&= \frac{k_bT}{6\pi a_{Eu}\mu} \quad && (T > Tm_{Fe_3O_4})
\end{aligned}
$$

Where D_0 is the pre-exponential factor, Q is the activation energy, k_b is the Boltzmann constant and a_{Eu} is the atomic size of Europium. It should be noted that the diffusive properties of oxide in steel with

the temperature are note very accurate. Nevertheless, as the dynamic is very fast the fluid transport is supposed to be more sensitive.

2.2.4 Liquid deformation and material ablation

In this model the liquid - gas interface has to move due to the recoil pressure compensated by surface tension and due to the material withdrawal by vaporization. The former phenomena is computed form pressure equilibrium coming from fluid flow calculation ($[AB]$ boundary condition in 2.2.2 paragraph), thus naturally conservative in mass. The last one is coming from the mass ablated rate calculation $\dot{m}$. As this mass leaves the studied system, it has to be uncorrelated to the mas conservation.

The following conditions describe the mesh motion on boundaries :

— at $[AE] \cup [ED] \cup [BF] \cup [FC]$ the boundaries are locked in the r direction and free in the z direction
— at $[DC]$ the boundary is free along r but z motion is set to zero
— at $[AB]$ the normal velocity of the boundary $\vec{v_b}$ is set to :

$$\vec{v_b}.\vec{n} = \vec{v}.\vec{n} - \vec{v_a}.\vec{n}$$

With $\vec{v}.\vec{n}$ the conservative part coming from the fluid flow calculation and $\vec{v_a}.\vec{n}$ the normal "ablation velocity" ($v_a = \dot{m}/\rho_m$)

The resulting motion of the mesh in the domains is computed in order to optimize the mesh quality. A not physical hyper-elastic model is used here.

2.2.5 Model and process parameters

The whole numerical problem is solved by the Finite Element Method with the commercial software *Comsol Multiphysics*.

The parameters used in previous models are summarized in table 1.

Properties	$304L$	Fe_3O_4	Common and Process Properties	$304L$ and Fe_3O_4
$\lambda \, [W/m/K]$	24.5	15	$\eta \, [Pa.s]$	0.004
$\rho \, [kg/m^3]$	8020	5180	$\sigma \, [N/m]$	1.6
$c_p \, [J/kg/K]$	609	621	$\frac{\partial \sigma}{\partial T} \, [N/m/K]$	1.210^{-4}
$D_0 \, [m^2/s]$	510^{-6}	4.710^{-7}	β_r	0.17
$\alpha \, [\%]$	29	70	$R_0 \, [m]$	32.510^{-6}
$A \, [cm^{-1}]$	3610^4	3210^4	$P_m \, [W]$	15
$T_m \, [K]$	1700	1863	$T_\infty \, [K]$	293
$T_v \, [K]$	3173	2896	$h_{cv} \, [W/m^2/K]$	10
$L_m \, [J/kg]$	2.610^5	610^5		
$L_v \, [J/kg]$	610^6	1.310^6		

TABLE 1 – Material and process parameters

2.3 Mesh and time step

This problem has the particularity to be dependent of different scales in space and in time. In other words, the oxide layer is 130 nm thick and the whole simulated piece is 30 μm thick (figure 1) and the pulse duration is 150 ns (figure 2) whereas the process period is 50 μs. Thus, the time and space discretizations have to be chosen carefully.

Firstly, in order to consider correctly the whole laser pulse, a time step of 5 ns is set during the pulse and 10 ns during the cooling. Secondly, the oxide layer is spatially meshed with triangular 10 nm elements. This size seems to allow correct computation of laser absorption and oxide concentration calculation. In the rest of the element sizes growth with a factor of 1.1.
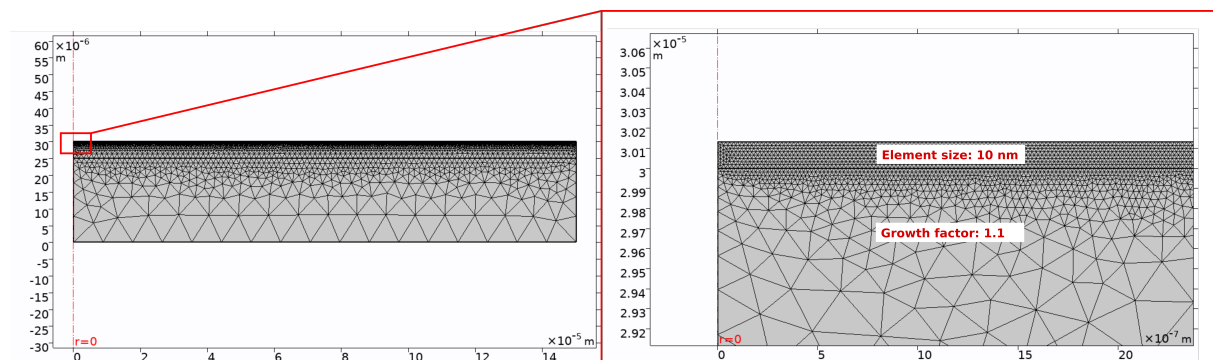
FIGURE 3 – Mesh illustration.

In order to reduce the Degrees Of Freedom to be solved, a linear interpolation is set in elements. The numerical problem is thus composed by more of 2500000 DOF, solved with 2x8@2.4GHz CPU in approximately 4 hours.

3 Results and discussions

Before presenting results, the aim of this numerical analysis has to be recalled. This model is made to predict the ablated material amount and to understand ablation phenomena. The first part of the results is the model validation regarding similar experiment. In a second step, the ablation phenomena will be analyzed in the current process parameter range.

3.1 Model validation

Firstly, the thermal field can be validated trough oxide ablation amount and melted zone comparisons with experiments. The figure 4 is an extrapolate 3D view showing oxide concentration decrease with the time during one spot laser processing. It can be observed that the ablated zone remains constant after 500 ns, i.e. few hundred nanoseconds after the laser pulse. Two mechanisms are responsible to the oxide amount decrease in the center part, the material removing due to evaporation and the fluid motion involved by recoil pressure.

The isolevel lines indicate the fusion and vaporization temperatures. The larger one can be compared to the experimental melted zone (figure 5).

In order to validate the thermal field, numerical key temperatures (melting and vaporization) are compared to experimental picture in figure 5. A particular caution have been taken to scales equality. The
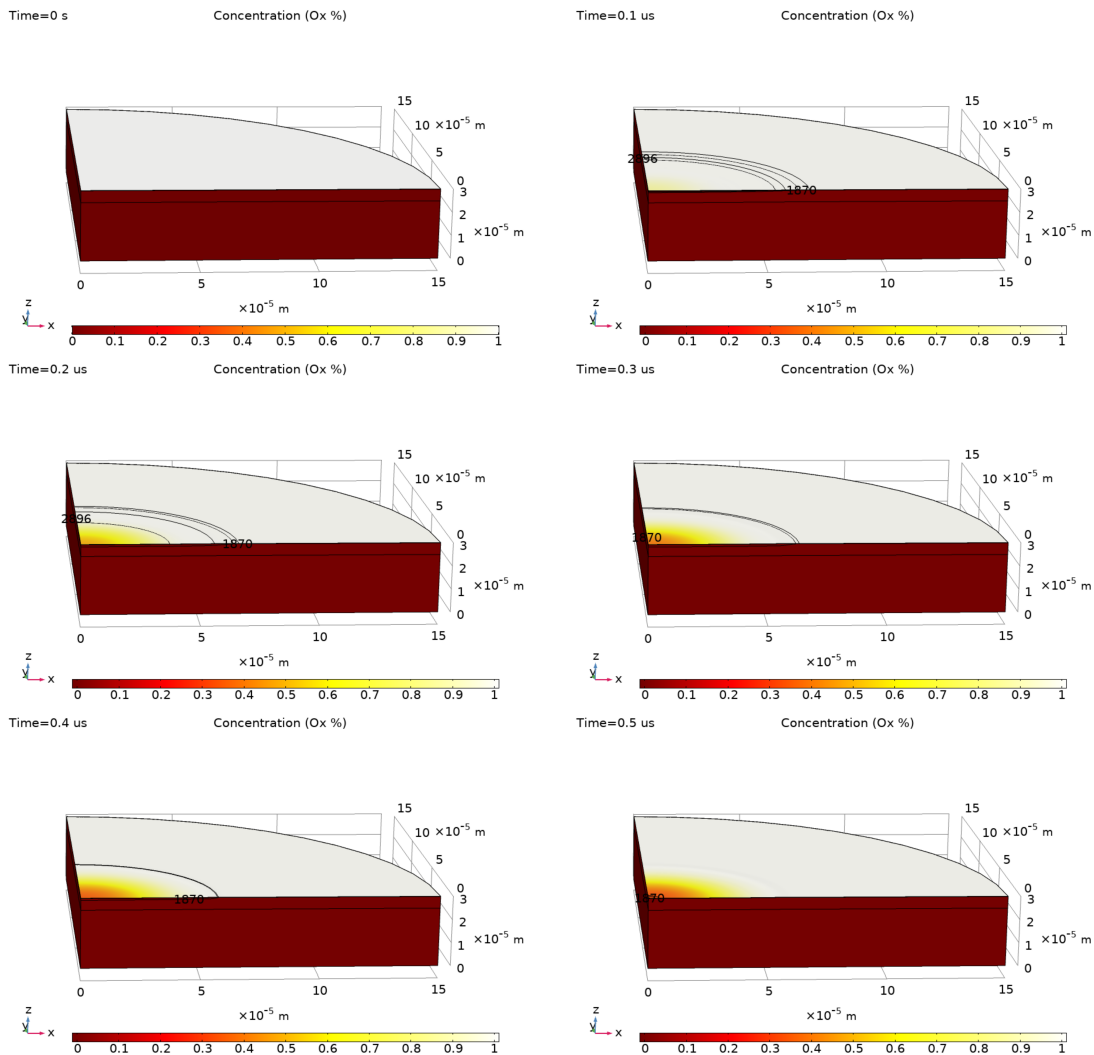
FIGURE 4 – Dynamics of oxide removal.

experimental picture shows three different areas, the ablated zone (lighter zone is the metal), oxide melted zone where the initial roughness seems to be modified and the solid oxide zone. The comparison indicated that the ablated zone corresponds to material part which is higher than the boiling point and the melted oxide limit is also consistent with calculated melted zone.

In addition to this upper view analysis, the melted thickness was measured on transmission electronic microscopy pictures. The experimental thickness is estimated to $0.7~\mu m$ whereas the numerical model predict $1.2~\mu m$. This discrepancy can be explained by the uncertainties on material properties at high temperature. Indeed, in the model, thermal properties are different for oxide and metal, but not temperature dependent. Moreover, as the phase change is very fast, it is quite difficult to detect the transition zone accurately on TEM pictures. The experimental information is probably slightly underestimated.

The computed minimal oxide residual concentration is close to $28~\%$. As the measured initial content of contaminant was $1~\%$ in the oxide we can estimate the its residual concentration as $0.28~\%$ numerically. This content has also been measured experimentally to $0.2~\%$ (by GDMS).

As the thermal and species fields are quite well estimated numerically, the model is supposed to be
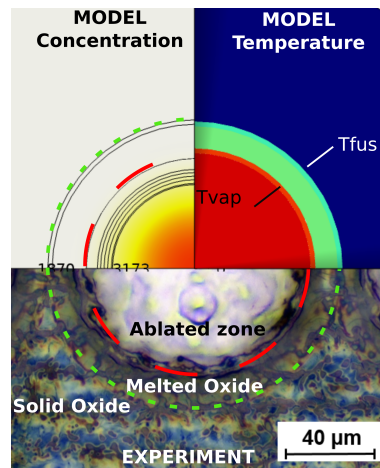
FIGURE 5 – Comparison experiment and numerical melted and evaporated zones

sufficiently predictive to allow understanding of the oxide layer withdrawal.

3.2   Oxide layer removal analysis

In this part, the previous model will be used to explain phenomena occurring during oxide layer ablation. The most probable reasons of oxide withdrawal are :

— phase explosion,
— mechanical fracturing,
— vaporization.

The first one appears when the metal start to evaporated before oxide with both oxide and metal in liquid phase. The second one is similar to glass cutting, i.e. the solid oxide is broken due to its thermal expansion. The last one, is the classical evaporation process, which means that the oxide leaves the sample as vapor.

To validate or invalidate one of the previous ablation origins, the temperature evolution seems to be crucial information. The time evolution of point A and E temperatures are plotted in figure 6. The different material melting and boiling points are added to the plot. The intersections of lines and temperature curves indicate when each phase start to melt and evaporate.

This figure indicates that the oxide melts and evaporates before metal. Moreover, the metal start to melt nearly when the oxide start to evaporate. When the metal start to evaporates, the calculated evaporation rate of oxide is more than 20 times higher than metal. This facts indicates that the phase explosion is the weakest likely assumption.

In addition to this analysis, the high evaporation rate indicates the vaporization is a sensitive phenomena in this context. For instance, for this case, with an evaporation radius equal to the laser beam radius (32 μm) during approximately $100\ ns$ the ablated mass during 1.4410^6 pluses (experimental conditions) is computed to $5.1\ mg$. The experimentally measured vaporized mass is estimated to $3.3\ mg$. The gap between these two values is mainly due to the context. Indeed, numerically, the ablated mass of one pulse is multiplied by the number of experimental spot while the experimental data concerns overlapped spots (80 %). Thus, the two evaporation cases are not perfectly similar, in the numerical case, only oxide is ablated, whereas in the experiment, a part of previously ablated area is reheated. As the oxide absorbs more energy than metal, the evaporation considered numerically is higher.
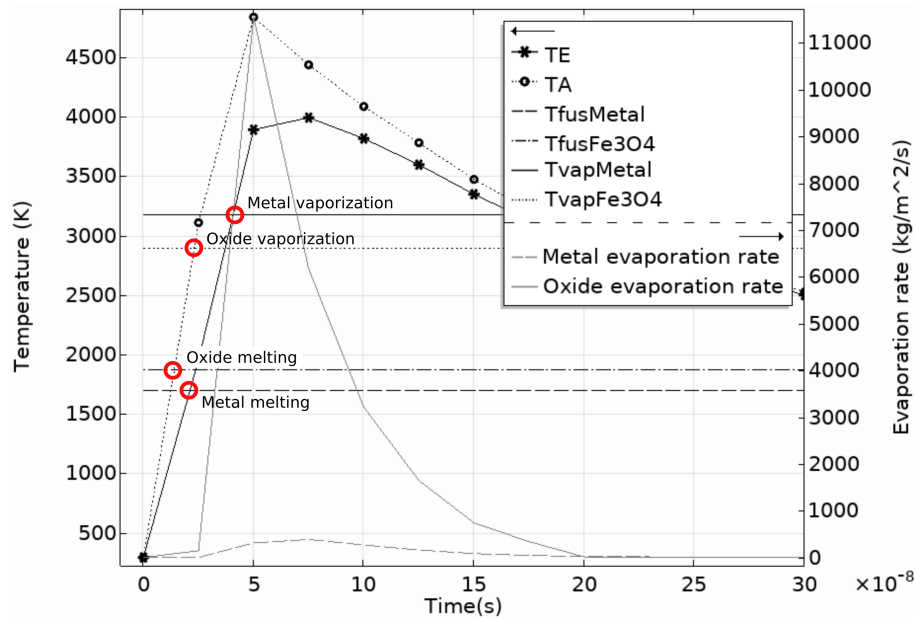
FIGURE 6 – Temperature and evaporation rate evolution with time on points A and E (Figure 1)

Without any mechanical model associated to the current simulation it is not possible to conclude numerically on mechanical fracturing, but as the ablated material was experimentally collected an observation of ejected particles can be made. A conclusion to these observations is that the particles present mainly spherical shape, more related to liquid or vapor phases. As a consequence, the vaporization phenomena seems to be the more plausible explanation for oxide withdrawal.

Références

[1] W.H. Kasner, T.A. Wojcik, H.E. Feree, Laser decontamination method, Patent EP0091646B1, 1986.

[2] S. Shuttleworth, M.R. Chandratillake, V.J. Robinson, Material removal by laser ablation, Patent WO1995027986A1, 1995.

[3] J.P Cartry, G. Clar, A. Martin, Apparatus for working by lasser, especially for the decontamination of a pipe of a nuclear reactor, US Patent 5,256,848, 1993.

[4] A. Leontyev, Laser decontamination and cleaning of metal surfaces : modelling and experimental studies, PhD thesis, Université Paris Sud - Paris XI, 2011.

[5] Ph. Delaporte, M. Gastaud, W. Marine, M. Sentis, O. Uteza, P. Thouvenot, J.L. Alcaraz, J.M. Le Samedy, D. Blin, Dry excimer laser cleaning applied to nuclear decontamination, Applied Surface Science, 208 (2003) 298–305.

[6] R.L. Demmer ,R.L. Ferguson, Testing and evaluation of light ablation decontamination, Technical report, EG and G Idaho, Inc., Idaho Falls, 1994.

[7] Nuclear Energy Agency, R& D and Innovation Needs for Decommissioning Nuclear Facilities, 2014.

[8] A.J. Potiens, J.C. Dellamano, R. Vicente, M.P. Raele, N.U. Wetter, E. Landulfo, Laser decontamination of the radioactive lightning rods, Radiation Physics and Chemistry, 95 (2014) 188–190.

[9] C. Bonacina, G. Comini, A. Fasano, M. Primicerio, Numerical solution of phase-change problems, International Journal of Heat and Mass Transfer, 16 (1973) 1825–1973.

[10] C.J. Knight, Theoretical modeling of rapid surface vaporization with back pressure, AIAA Journal, 17 (1979) 5p.

[11] A. Matsunawa , V. Semak, The simulation of front keyhole wall dynamics during laser welding, Journal of Physics D : Applied Physics, 30 (1997) 798–809.

[12] K. Hirano, R. Fabbro, M. Muller, Experimental determination of temperature threshold for melt surface deformation during laser interaction on iron at atmospheric pressure, J. Phys. D. Appl. Phys., 44 (2011) 435402.

[13] A.A. Samokhin, Effect of Laser Radiation on Absorbing Condensed Matter, Nova Science Publishers, (1990).

[14] A.D. Pasternak, D.R. Olander., Diffusion in liquid metals, AIChE Journal, 13(6) (67) 1052–1057.